Electrochemical Measurement of Velocity Gradient at the Wall of a Helical Tube

Sylvain Galier, Sébastien Issanchou, Philippe Moulin, Michael J. Clifton and Philippe Aptel
Laboratoire de Génie Chimique (CNRS UMR 5503), Université Paul Sabatier, 31062 Toulouse Cedex, France

An electrochemical technique was used for measuring the wall velocity gradient in two coiled pipes: a torus and a helix. An electrochemical oxidation reaction was employed with its rate limited by mass transfer. Measurement of the diffusion-limited current at a microelectrode embedded flush with the wall allows the wall shear rate to be determined. The flow velocity was varied through both the laminar and turbulent regimes. Measurements were made for different electrode positions on the pipe circumference and, as expected, the highest shear rate was found at the outside of the curve, with the lowest value at the inside. In the case of the helical pipe, maxima and minima in shear rate were shifted slightly away from the positions observed for the torus.

Introduction

Concentration polarization and membrane fouling are severe limitations for mass transfer in membrane-based separation processes, especially in the production of drinking water. Process productivity is reduced because of the resulting decrease in permeate flux and, in order to maintain good performance, back-washing is necessary. However, backwash frequency and efficiency are variable and have an impact on water recovery. Special flow patterns can be useful in overcoming concentration polarization (Winzeler and Belfort, 1993; Belfort et al., 1994) and various possibilities have been tested: turbulent flow, baffles, or inserts (Gupta et al., 1995; Wang et al., 1994), pulsations (Ding et al., 1991; Wang et al., 1994), rotating membrane filters (Taylor vortex flow) (Park et al., 1994), and secondary flow (Dean flow) (Tanishita et al., 1975; Brewster et al., 1993; Moulin et al., 1996a, 1999)

In membrane filtration performed with hollow-fiber membranes, the helical configuration enhances the permeate flux and decreases the backwash frequency in comparison with a straight configuration. This improvement in process efficiency is due to the presence of secondary flows that increase the wall shear stress. The advantage of using helical membranes compared with other devices is the ease with which straight hollow fibers can be wound into a helix without reducing the membrane area per unit volume of equipment (Guigui, 2000).

Moulin et al. (1996a, 1999) have measured the performance of membrane filtration with helically wound hollow-fiber membranes. Comparison was made between the mass-transfer enhancement obtained in using helical tubes and the accompanying increase in pressure drop. These studies pointed out a proportional relationship between the permeate flux and the increase in wall shear stress. Furthermore, for a given permeate flow rate, the energy consumption is lower in the helical configuration than in a straight one (Ghogomu et al., 2001).

In membrane processes any nonuniformity in mass transfer rate can have undesirable effects. If mass transfer is less effective on some parts of the membrane, there will be a tendency for these zones to be fouled or blocked, thus reducing the useful membrane area and imposing more frequent backwash. To obtain a clearer view of mass transfer in Dean flows in helical tubes, it was decided to perform local measurements so as to obtain more information on wall shear rate than can be reached by overall measurements such as pressure drop.

Reiss and Hanratty (1962, 1963) proposed an electrochemical method to study turbulent flow close to a wall. Hanratty and Campbell (1983) used the same approach to measure the local velocity gradient at a wall. This is the technique used in the present work. It consists in measuring the diffusion-limited current on a small polarized electrode embedded in the wall flush with its surface. A fast redox reaction is used so that the limiting current really measured corresponds to the rate of diffusion to the electrode surface. Furthermore,

Correspondence concerning this article should be addressed to S. Galier.
Current address of P. Moulin: Laboratoire en Procédés Propres et Environnement (LPPE-EA-884), ENSSPICAM, Domaine Universitaire de Saint Jérôme, Av. Escadrille Normandie Niemen, 13397 Marseille Cedex 20, France.

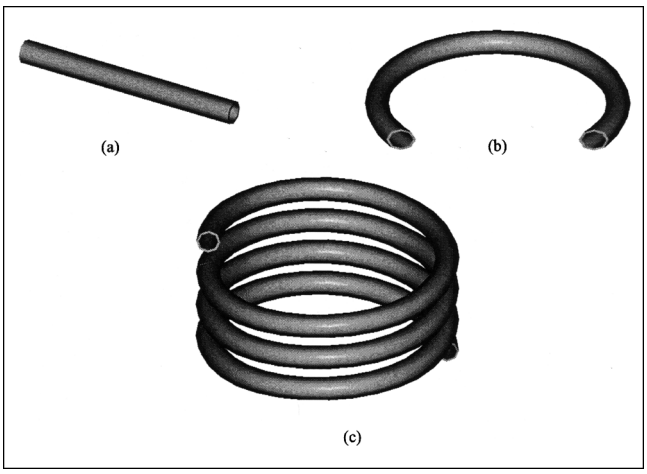

Figure 1. Geometries studied: (a) straight; (b) torus; (c) helical.

the electrode can be made small enough in comparison with the pipe diameter for the measurements to be considered as local ones. The technique was calibrated using chronoamperometry to determine the electrode surface area. In the present study, different electrode positions on the pipe circumference were used and measurements were performed at various values of the Reynolds number. Three pipe geometries were used: a straight pipe, a torus, and a helix that served to check the effect of the pitch of the coil (Figure 1). A comparison between the experimental results and the theoretical values for a straight pipe makes it possible to check the accuracy of the technique used.

Theory

Secondary flows in curved pipe

The secondary flows that appear orthogonally to the main flow in a curved pipe are caused by centrifugal force: the fast-flowing liquid near the center of the pipe is driven towards the wall on the outside of the curve, while the slow-moving liquid near the wall flows back towards the inside of the curve (Figure 2). Thus two counter-rotating roll-cells appear; these are known as Dean roll-cells. Dean (1927, 1928) first studied this complex flow pattern in a curved pipe using a coaxial toroidal coordinate system. He showed that the parameter *De*, now known as the Dean number, is the parameter governing fluid motion in such a pipe

$$De = Re\sqrt{\frac{d_i}{d_c}} \tag{1}$$

where Re is the Reynolds number, d_i is the inner pipe diameter, and d_c is the coil diameter. These flows are accompanied by a deformation in the profile of the axial flow: its maximum shifts away from the central line of the pipe towards the outer wall as the flow rate increases. Dean roll-cells are present even at the lowest Dean numbers: at higher Dean numbers, a centrifugal instability appears close to the concave outer wall of the tube and generates another pair of

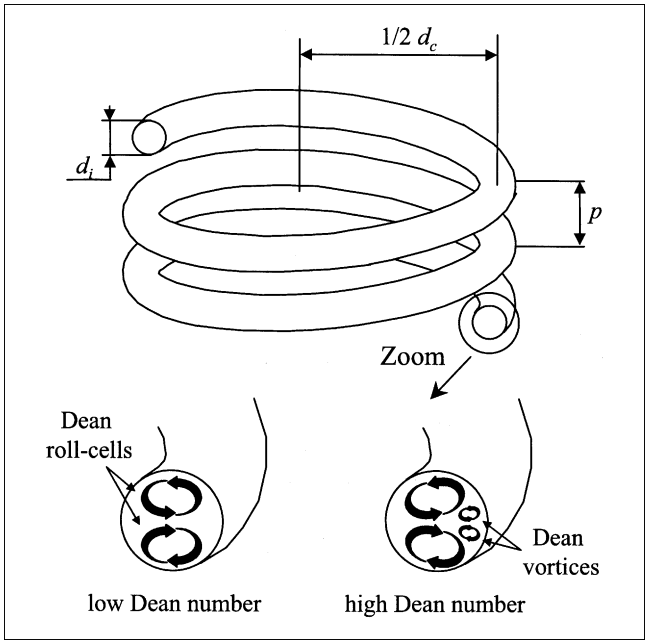

Figure 2. Dean vortices in a coiled pipe.

counter-rotating vortices known as Dean vortices. While the roll-cells occupy almost the whole cross-section, the Dean vortices occupy only a small part of it (Figure 2).

In the case of a helical pipe of pitch p a modified Dean number is used

$$De' = Re\sqrt{\frac{d_i}{d'_c}} \tag{2}$$

where d'_c is the effective coil diameter, taking into account the curvature due to the torsion

$$d'_c = d_c\left[1+\left(\frac{p}{\pi d_c}\right)^2\right] \tag{3}$$

The critical Reynolds number Re_c, which fixes the limit between the laminar and turbulent regimes, is given by the relationship (Mishra and Gupta, 1979)

$$Re_c = 2\times 10^4\left(\frac{d_i}{d_c}\right)^{0.32} \tag{4}$$

This relationship is valid for the range of values: $0.003 < d_i/d_c < 0.15$ and $0 \le p/d_c < 25.4$.

Wall velocity gradient - friction factor - shear stress in a pipe

For a Newtonian fluid, the velocity gradient $\dot{\gamma}$ is proportional to the shear stress τ

$$\dot{\gamma} = \frac{\tau}{\mu} \tag{5}$$

where μ is the dynamic viscosity.

For flow in a pipe, the friction factor ($f/2$) is usually defined by wall shear stress τ_w

$$\tau_w = (f/2)\rho v^2 \tag{6}$$

where ρ is the fluid density and v the mean fluid velocity.

So, the velocity gradient $\dot{\gamma}$ at the wall is linked to the friction factor by the relationship

$$\gamma = \frac{v^2(f/2)}{\nu} \tag{7}$$

Straight Pipe. In the case of laminar flow ($Re < 2{,}100$), the friction factor ($f/2$) is obtained from the Hagen-Poiseuille law

$$(f/2)_s = \frac{8}{Re} \tag{8}$$

For turbulent flow, several relationships have been established empirically for different ranges of Re and make it possible to calculate ($f/2$) from the Reynolds number (Moulin et al., 2001). The expression used in this study is the Blasius correlation

$$(f/2)_s = 0.0395 Re^{-0.25} \tag{9}$$

for $Re > 3{,}000$.

Torus and Helical Coiled Pipe. Mishra and Gupta (1979) devised empirical correlations for the friction factor in coiled pipes, for both laminar and turbulent regimes, based on measurements of the pressure drop. Their relationships are valid within the same range of geometrical parameters as for Eq. 4: $0.003 < d_i/d_c < 0.15$ and $0 \le p/d_c < 25.4$. For the laminar regime, their formula gives the ratio of the friction factor in a coiled pipe to that in a similar straight one

$$\frac{(f/2)_c}{(f/2)_s} = 1 + 0.033\,(\log_{10} De')^4 \tag{10}$$

The same authors also give a corresponding equation for turbulent regime ($Re > Re_c$)

$$(f/2)_c = (f/2)_s + 0.00375\left(\frac{d_i}{d_c}\right)^{0.5} \tag{11}$$

Wall velocity gradient measurement using an electrochemical method

Microelectrodes are a traditional means for measuring local wall shear rates. The electrodes used here are circular with a diameter of about one millimeter. Figure 3 shows such an electrode embedded flush with an inert wall.

The method is based on the electrochemical reaction of a species at the test electrode (the microelectrode). As the electrode voltage is raised above the equilibrium value, the reaction rate increases until it becomes limited by the mass transfer. The concentration of the reacting species (the electroactive species) is then zero at the electrode surface. Under these conditions, the current measured, called the limiting current, is fixed by the rate of mass transfer. The choice of the electroactive species must satisfy various requirements: the most commonly used reaction is the reduction of ferricyanide (Sutey and Knudsen, 1969; Jenkins and Gay, 1977)

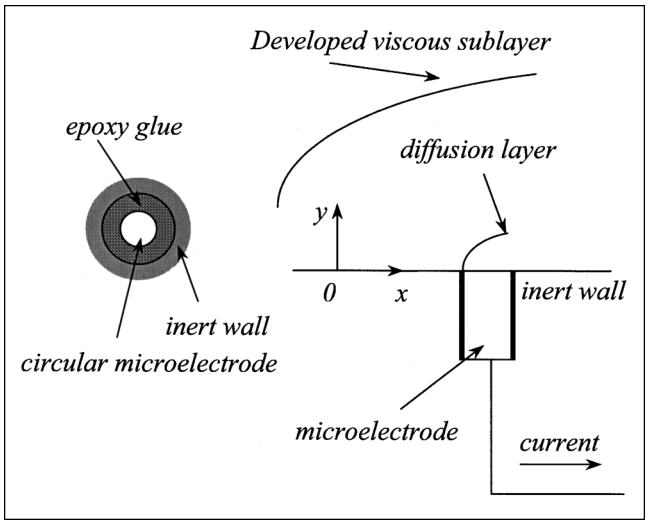

Figure 3. Principle of a microelectrode embedded flush in an inert wall.

$$Fe(CN)_6^{3-} + 1e^- \rightarrow Fe(CN)_6^{4-}$$

To eliminate the effect of ionic migration, the electroactive species is diluted in an excess of supporting electrolyte. So the mass-transfer mechanisms involved in the system are molecular diffusion and convection in the x direction. As the electrode diameter is small in comparison with the pipe radius, the surface curvature can be neglected and a Cartesian geometry can be used. The continuity expression for the concentration of electroactive species under steady-state conditions is given by the convection-diffusion equation

$$v_x \frac{\partial c}{\partial x} = D\left[\frac{\partial^2}{\partial x^2} + \frac{\partial^2}{\partial y^2} + \frac{\partial^2}{\partial z^2}\right] c \tag{12}$$

Since the diffusion-layer thickness is small in comparison with the pipe radius and the electrode diameter is small enough, it is possible to approximate the axial velocity by a linear function of the distance from the surface

$$v_x = \gamma y \tag{13}$$

where γ is the velocity gradient (shear rate) at the wall.

The limiting conditions for this equation are that the concentration of the electroactive species far from the electrode is everywhere c_0, while on the circular surface of the electrode the reaction is fast enough for the concentration to be zero. On the wall outside the electrode area, the concentration gradient perpendicular to the wall is zero: $\partial c/\partial y = 0$. The x axis can be taken as passing through the center of the

electrode; then, there is a symmetry condition about the x-O-y plane: $c(x,y,z) = c(x,y,-z)$.

Use of dimensionless variables allows a reduction in the number of parameters

$$\hat{c} = c/c_0; \left[\hat{x}, \hat{y}, \hat{z}\right] = \left[x/d, y/d, z/d\right]; Pe = d^2\gamma/D$$

Thus, after the substitution of Eq. 13 and the introduction of the dimensionless variables, Eq. 12 becomes

$$\hat{y}\frac{\partial \hat{c}}{\partial \hat{x}} = \frac{1}{Pe}\left[\frac{\partial^2}{\partial \hat{x}^2} + \frac{\partial^2}{\partial \hat{y}^2} + \frac{\partial^2}{\partial \hat{z}^2}\right]\hat{c} \tag{14}$$

The quantity related to the measurable current is the average mass-transfer flux of the electroactive species to the electrode surface. This in turn can be related to the bulk concentration of electroactive species using a mass-transfer coefficient

$$\frac{4}{\pi d^2}\frac{I_{\lim}}{\nu_e F} = \langle J \rangle = -D\left\langle \frac{\partial c}{\partial y} \right\rangle = kc_0 \tag{15}$$

The mass-transfer coefficient k can be conveniently expressed as a Sherwood number

$$Sh = kd/D \tag{16}$$

In this way the whole problem can be reduced to determining the functional relationship between Sh and Pe.

Mollet et al. (1974) integrated the above system of equations, neglecting diffusion in the x and z directions. The results of their calculations can be represented by the relationship

$$\dot{\gamma} = \frac{3.211}{d^5 D^2}\left(\frac{I_{\lim}}{\nu_e F c_0}\right)^3 \tag{17}$$

or in dimensionless form

$$Sh = 0.863 Pe^{1/3} \tag{18}$$

The validity of neglecting the contribution of these two terms to diffusion is not obvious, particularly in the case of very small electrodes. In order to check the impact of this approximation, Eq. 14 was solved numerically on a three-dimensional (3-D) grid (204 x steps, 80 y steps and 50 z steps) using a common finite-volume technique developed by Patankar (1980). In this way the three-dimensional concentration distribution of electroactive species is obtained for the volume close to the electrode; averaging the concentration gradient over the electrode surface gives the mass-transfer coefficient at the electrode. The results of this calculation can be expressed as

$$Sh = K\, Pe^{1/3} \tag{19}$$

In Figure 4 the parameter K is plotted as a function of the Péclet number over the range of values used in this work. It can be seen that K is somewhat higher than the value of 0.863 at low Pe, but tends towards this value at higher values of Pe. This variation is in agreement with the intuitive understanding of the physical system: diffusion in the x and z directions should begin to play a role for small electrodes and low values of the velocity gradient, that is, at low Pe. However, as the deviations from Eq. 18 are not very great, this relationship was used for the sake of simplicity throughout the rest of this work.

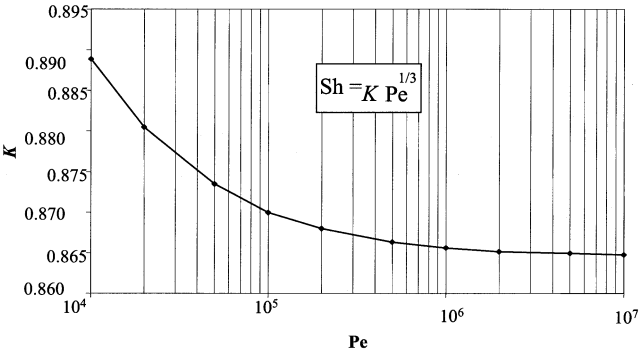

Figure 4. Variation of the coefficient K with the Péclet number.

Experimental Arrangement

The characteristics of the torus and the helical coiled pipe used in our experiments are given in the Table 1; they lie within the range of validity of the correlations of Mishra and Gupta (1979) (Eqs. 10 and 11). The channel dimensions are such that the flow is always fully developed at the outlet of the coil where the measurements are performed. Wolff and Cognet (1985) measured local mass-transfer rates in a 180° bend. Their results show apparently irregular variations. However, these could be due to the fact that the flow within this short channel is still developing. Applying the correlation of Austin and Seader (1973) to their results shows that flow is fully developed at the outlet of the bend only at low Reynolds numbers ($Re < 300$).

The experimental arrangement used in this work is shown in Figure 5. The electrolyte is pumped from a closed tank and saturated with nitrogen before and during the experiments in order to avoid a side reaction: the reduction of dissolved oxygen. The electrolyte is maintained under agitation and its temperature is controlled with a heat exchanger, so the solution properties (D, ρ, μ) are constant. The feed pump and a bypass allow a controlled circulation to be maintained and the flow rate is measured using an electromagnetic flow meter.

Table 1. Characteristics of Pipes

	Straight Pipe	Torus	Helical Coiled Pipe
Internal pipe dia. d_i (mm)	10	10	10
Coil dia. d_c (mm)	—	270	270
Re_c	2,000	6,966	6,966
Pitch p (mm)	—	0	12
Length	1 m	320°	450°

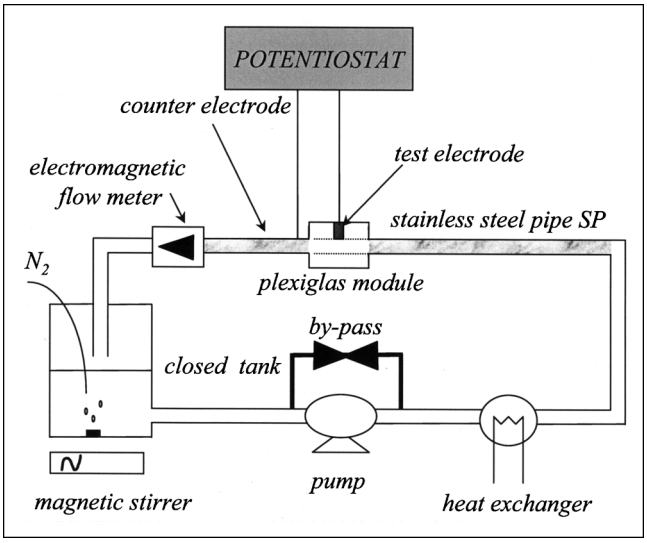

Figure 5. Experimental arrangement.

The potential between the test electrode and the downstream counterelectrode is controlled by a potentiostat. The electrochemical reaction rate is limited by mass transfer when a suitable potential is applied (-0.60 V vs. saturated-calomel electrode). In this way measurement of the diffusion-limited current allows the wall velocity gradient to be determined (Eq. 17). The counterelectrode is a stainless-steel pipe: it has a much larger surface area than the test electrode. So, under normal operating conditions, the reference voltage is constant and the electrochemical reaction at the test electrode is not limited by the reaction at the counterelectrode.

The test electrode is a platinum wire (dia. 0.5 mm) embedded in a Plexiglas tube, fixed in place by an epoxy resin and made flush with the wall (Figure 6). The electrode assembly was situated at the outlet of the coiled section of tubing after a very short length of straight tube; it could be rotated to allow measurements at different angles. A fixed dial marked every 10° was used, together with a pointer attached to the electrode assembly, to fix the angular position of the electrode to within $\pm 1°$. The test electrode was cleaned in two steps: first polishing on felt with diamond paste to remove any oxide coating, then cathodic cleaning in 0.5 mol L^{-1} sodium hydroxide at -1.64 V vs. saturated-calomel electrode for 10–20 min.

As mentioned above, the electrochemical reaction used is the reduction of ferricyanide. The electrolyte solution contains equimolar concentrations of potassium ferricyanide and potassium ferrocyanide at 5×10^{-3} mol L^{-1} with 0.5 mol L^{-1} sodium hydroxide. The diffusion coefficient of the electrolyte was checked experimentally using a rotating-disk electrode and the value found was: $D = 6.0 \times 10^{-10}$ m^2 s^{-1}. The kinematic viscosity of the electrolyte solution at 20°C was measured with a capillary viscometer: $\nu = 1.08 \times 10^{-6}$ m^2 s^{-1}.

Results and Discussion

Electrode diameter

The test electrode surface area must be accurately measured, so constant potential chronoamperometry was used.

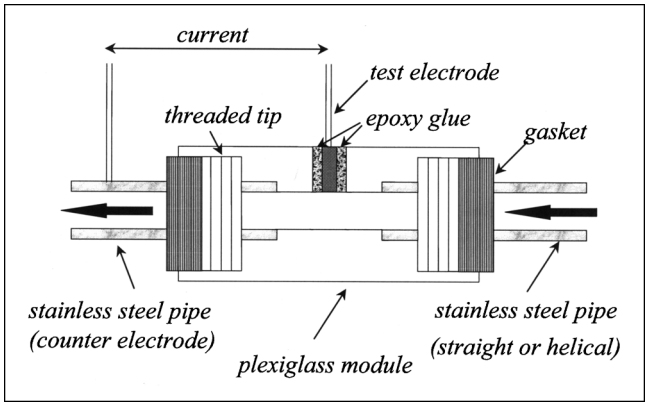

Figure 6. Plexiglas support module and test electrode.

This electrochemical technique consists in measuring, as a function of time, the limiting current, that is, the current obtained for an imposed potential such that the concentration of the electroactive species at the electrode surface is zero. For a flat electrode in an unstirred solution and for a sufficiently short time period, the variation of current with time is given by the Cottrell equation (Bard and Faulkner, 1980)

$$I_{\text{lim}} = \frac{\nu_e F A D^{1/2} c_o}{\pi^{1/2} t^{1/2}} \tag{20}$$

The measurements have to be performed over a short time period to avoid the formation of density gradients that could generate natural convection and so modify the limiting current. In Eq. 20, A is the electrode surface area that can be determined from the slope of the plot of I_{lim} vs. $t^{-1/2}$. The electrode diameter was found to be 0.575 mm.

Straight pipe

The wall velocity gradient measured using the electrochemical technique with the straight pipe is plotted (with the theoretical values) as a function of the Reynolds number in Figure 7a for the laminar regime and in Figure 7b for the turbulent regime. The experimental results are consistent with theoretical values given in the laminar (Eqs. 7 and 8) and turbulent regimes (Eqs. 7 and 9).

Coiled pipe

Dean Flow Effects and Influence of the Pitch. To determine the distribution of velocity gradient at the wall, measurements were carried out for different electrode positions on the torus circumference. Figure 8 gives experimental values for $Re = 3{,}240$ (laminar regime): the ratio of the wall shear rate for a helical tube to that for the straight tube γ_c/γ_s is plotted as a function of the angular position on the pipe circumference, for two different values of the pitch (0 for the torus and 12 mm for the helical tube). The velocity gradient is highest at the outer wall of the pipe (0° or 360°) and is lowest at the inner wall (near 180°).

In the case of a helical or toroidal configuration, the Dean roll-cells stabilize the flow in the tube and the transition be-

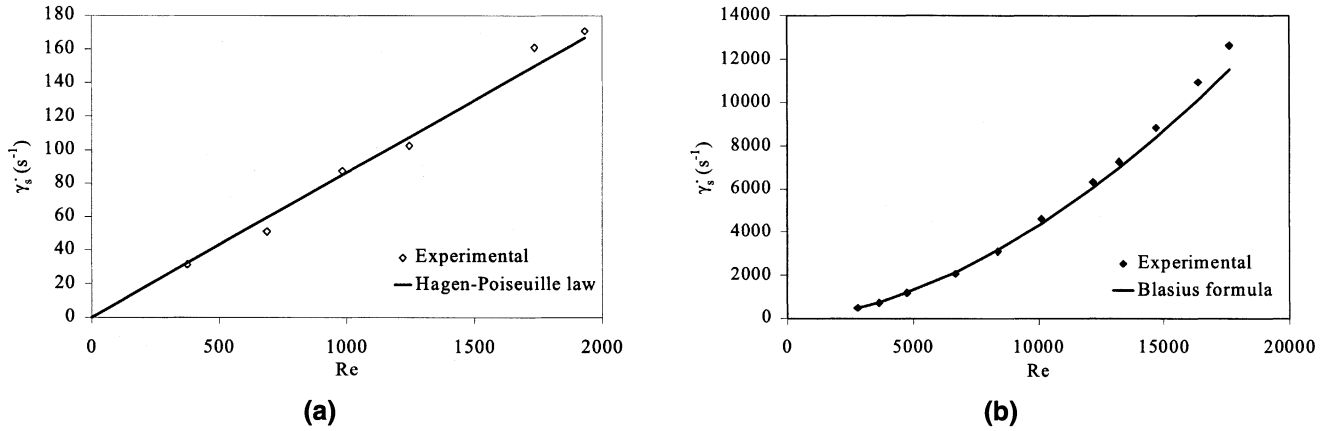

Figure 7. Experimental and theoretical wall velocity gradients vs. Reynolds number in the straight pipe. (a) laminar regime, (b) turbulent regime.

tween laminar and turbulent regimes is shifted to a higher value than for a straight tube. To assess this transition Reynolds number, wall velocity gradients were measured for different Reynolds numbers in straight and helical tubes (Moulin, 1996b). The transition to turbulence was identified by an abrupt change in slope: this appears at a Reynolds number around 2,100 for a straight tube and at a higher value for a helical tube. These observations are in qualitative agreement with those of Castelain et al. (1997).

The wall shear rate in the torus is compared in Figure 8 with its value in the helical coiled pipe under the same conditions. For the torus, the maximum velocity gradient is at 0° and the minimum is slightly below 180°. For the helical coiled pipe, Germano (1982, 1989) and Wang (1981) observed that the pitch of the coil displaces both the maximum and minimum in the velocity gradient. Moll et al. (2001, 2002) also found by numerical simulation that the pitch of the coil modifies the position of the maximum in wall velocity gradient. In the results of the present experimental work shown in Figure 8 the minimum is clearly displaced away from the 180° angle, but the maximum is not noticeably displaced. This is because the electrochemical method does not allow the position of the maximum to be determined precisely: the curve at that point is quite flat and the range of values of the pitch in this study (from 0 to 12 mm) is narrower than that used in the numerical study by Moll et al. (from 0 to 150 mm).

Effect of Flow Regime. For the straight pipe and the helical coil, the Reynolds number was set at various values up to 10,020: this range covers the laminar and turbulent regimes for both geometries. Figure 9 shows the ratio of the wall velocity gradient in the helical pipe to that in the straight pipe as a function of the angular position on the pipe circumference for different Reynolds numbers.

There are interesting aspects to be noted in these results:

• For $Re < 2{,}000$, the regime is laminar in both geometries. The wall velocity gradient is higher at all angles in the helical pipe than in the straight one. However, the effect of the Dean flow is greater on the outer wall (at 0° or 360°, $\gamma_c/\gamma_s = 2.5$) than on the inner wall (at 180°, $\gamma_c/\gamma_s = 1.4$). This reflects the structure of the Dean roll-cells: the highest shear rate is located where the flow is towards the wall and the lowest where the flow is away from the wall. The mean value of 2.0 is in agreement with the correlation of Mishra and Gupta (1979).

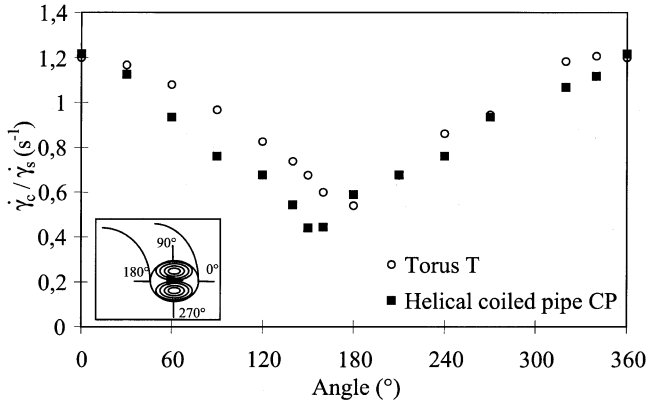

Figure 8. Ratio of the wall velocity gradients for different positions in the torus (pitch = 0) and the helical coiled pipe (pitch = 1.2 cm) for *Re* = 3,240.

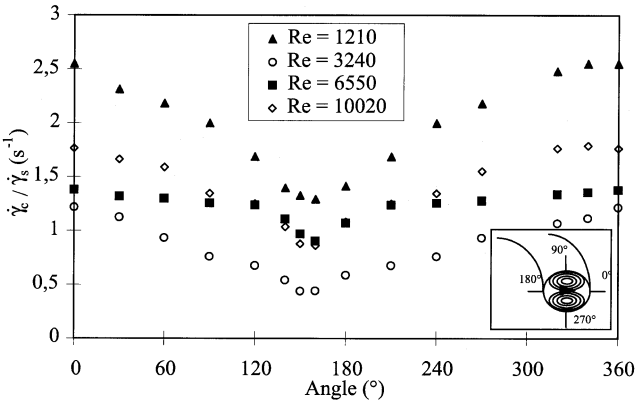

Figure 9. Ratio of the wall velocity gradients for different position in the coiled pipe for different values of *Re*.

• For 2,200 < Re < Re_c, the flow is turbulent in the straight pipe and laminar in the helically coiled pipe, and the ratio γ_c/γ_s is lower than for the previous range of Reynolds number. At a Reynolds number of 3,240, there is still a marked difference between the velocity gradients at the outer wall (0° or 360°) and at the inner wall (180°), but the mean ratio is close to 1, so that the Dean flow has about the same overall effect as turbulent flow at this value of Re. In this range, the effect of turbulent flow on the wall shear stress in a straight tube "compensates" for the effect of Dean roll-cells in the curved one. In the case of laminar flow, the ratio of the average shear stress in a coiled tube to that in a straight tube increases with increasing Reynolds numbers up to Re = 2,000. Beyond Re = 2,000, the flow remains laminar in the helical pipe, but becomes turbulent in the straight pipe and the ratio decreases. This is consistent with the results published by Moulin et al. (2001).

• At Re = 6,550, the Reynolds number is close to the critical value (Re_c = 6,966) for the helical pipe and the flow is turbulent in the straight pipe. The ratio γ_c/γ_s varies little with the angle of measurement, thus suggesting a modification in the flow pattern in the helical pipe.

• For Re = 10,020, ($Re > Re_c$) the flow is turbulent in both geometries, the ratio γ_c/γ_s increases above the previous values, but it remains lower than for Re < 2,000. The variation with measurement angle is once again quite marked, thus showing the effect of centrifugal force, that is, Dean flow effect, even in the turbulent regime. Similar results are obtained by Ligrani and Hedlund (1998) in heat transfer. They say that "Dean vortex pairs are not only present in the channel at small Dean numbers, but they also strongly influence thermal flow field behavior, even when the curved channel flow is fully turbulent."

Comparison with Pressure-Drop Correlations. The Mishra and Gupta correlations based on pressure-drop measurements in curved pipes allow the friction factor to be calculated for both flow regimes. Figure 10 shows the average of the experimental velocity gradients at the wall as a function of the value calculated from the Mishra and Gupta correlations. The experimental velocity gradient is a mean value calculated from the measurements made at different positions on the pipe circumference. It is in good agreement with the values given by the correlations. Like the numerical simulation presented by Moulin et al. (2001), the present results represent an important improvement over the Mishra and Gupta correlations that only give mean values.

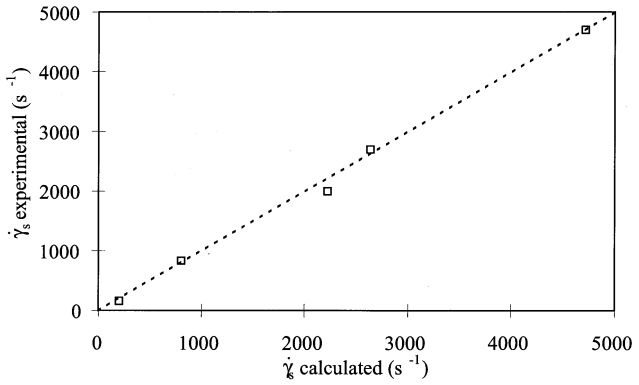

Figure 10. Measured wall velocity gradients in a torus vs. calculated from the correlation of Mishra and Gupta (1979) (for *Re* = 1,210, 3,240, 6,550, 7,220, 10,020).

Conclusion

The electrochemical method used in this work was found to be suitable for measuring the wall velocity gradient in a pipe. It was applied to measuring the distribution of velocity gradient at the wall in a torus and in a helical pipe. In both cases the velocity gradient is higher at the outer wall of the curved pipe and lower at the inner wall. The effect of the pitch of the helical pipe is to shift the maximum and minimum in wall shear rate away from the points lying on the coil diameter (0° or 360° and 180°). However, the shift in the maximum is not clearly visible in the present results.

With this method, it was possible to quantify the improvement in the wall velocity gradient in a helical coiled pipe compared with a straight one. For a given cross-flow velocity, the shear rate improvement due to the use of a helical pipe in comparison with a straight pipe is greater for the laminar regime.

Acknowledgments

The authors wish to thank Jean-Christophe Rouch for his help in building the experimental setup and Alain Bergel for many helpful discussions. The Pr. Gérard Cognet is also sincerely acknowledged for his help and for useful discussions.

Notation

A = electrode surface area
c = concentration of electroactive species
c_0 = bulk concentration
$\hat{c}$ = dimensionless concentration
d = electrode diameter
d_i = inner pipe diameter
d_c = coil diameter
d'_c = effective coil diameter
D = diffusion coefficient
De = Dean number
De' = Dean number modified by the pitch
$f/2$ = friction factor
F = Faraday constant
$I_{\lim}$ = diffusion-limited current
$\langle J \rangle$ = mean solute flux
k = mass-transfer coefficient
K = coefficient in mass-transfer correlation
p = pitch of the coil
Pe = Peclet number, $d\gamma^2/D$
Re = Reynolds number, $\upsilon\, d_i/\nu$
Re_c = critical Reynolds number
Sh = Sherwood number, kd/D
υ = mean fluid velocity
υ_x = axial velocity component
x,y,z = co-ordinates
$\hat{x},\hat{y},\hat{z}$ = dimensionless co-ordinates

Greek letters

γ = velocity gradient at the wall
μ = dynamic viscosity
ν = kinematic viscosity, μ/ρ
ν_e = number of electrons involved in the electrochemical reaction
ρ = fluid density
τ = shear stress

Subscripts

c = coiled
s = straight
w = wall

Literature Cited

Austin, L. R., and J. D. Seader, "Fully Developed Viscous Flow in Coiled Circular Pipes," *AIChE J.*, **19**, 85 (1973).

Bard, A. J., and L. R. Faulkner, *Electrochemical Methods, Fundamentals and Applications*, Wiley, New York (1980).

Belfort, G., R. B. Davis, and A. L. Zydney, "The Behavior of Suspensions and Macromolecular Solutions in Crossflow Microfiltration," *J. Memb. Sci.*, **96**, 1 (1994).

Brewster, M. E., K. Y. Chung, and G. Belfort, "Dean Vortices with Wall Flux in a Curved Channel Membrane System: 1: A New Approach to Membrane Module Design," *J. Memb. Sci.*, **81**, 127 (1993).

Castelain, C., A. Mokrani, P. Legentilhomme, and H. Peerhossaini, "Residence Time Distribution in Twisted Pipe Flows: Helically Coiled System and Chaotic System," *Exper. Fluids*, **22**, 359 (1997).

Dean, W. R., "Note on the Motion of Fluid in a Curved Pipe," *Philos. Mag.*, **4**, 208 (1927).

Dean, W. R., "The Stream Line Motion of Fluid in a Curved Pipe," *Philos. Mag.*, **5**, 673 (1928).

Ding, L. H., C. Charcosset, and M. Y. Jaffrin, "Albumin Recovery Enhancement in Membrane Plasma Fractionation Using Pulsative Flow," *Int. J. Artificial Organs*, **14**, 61 (1991).

Germano, M., "On the Effect of the Torsion in a Helical Pipe Flow," *J. Fluid Mech.*, **125**, 1 (1982).

Germano, M., "The Dean Equations Extended to a Helical Pipe Flow," *J. Fluid Mech.*, **203**, 289 (1989).

Ghogomu, J. N., C. Guigui, J. C. Rouch, M. J. Clifton, and P. Aptel, "Hollow-Fibre Membrane Module Design: Comparison of Different Curved Geometries with Dean Vortices," *J. Memb. Sci.*, **181**, 71 (2001).

Guigui, C., "Procédé Hybride de Coagulation/Ultrafiltration pour la Potabilisation des Eaux de Surface," PhD Thesis, Université Paul Sabatier, Toulouse, France (2000).

Gupta, B. B., J. A. Howell, D. Wu, and R. W. Field, "Helically Baffled Cross Flow Microfiltration," *J. Memb. Sci.*, **99**, 31 (1995).

Hanratty, T. J., and J. A. Campbell, "Measurement of Wall Shear Stress," *Fluid Mechanisms Measurements*, R. J. Goldstein, ed., Hemisphere, Washington, 559 (1983).

Jenkins, J. D., and B. Gay, "Experience in the Use of the Ferri-Ferrocyanide Redox Couple for the Determination of the Transfer Coefficients in Models in Shell Band Tube Heat Exchangers," *Euromech. 90 Proc.*, Session IIIc, 1 (1977).

Ligrani, P. M., and C. R. Hedlund, "Transition to Turbulent Flow in Curved and Straight Channels with Heat Transfer at High Dean Numbers," *Int. J. Heat Mass Transfer*, **41**, 1739 (1998).

Mishra, P., and S. Gupta, "Momentum Transfer in Curved Pipes," *Ind. Eng. Chem. Proc. Des. Dev.*, **18**, 130 (1979).

Moll, R., D. Veyret, P. Moulin, and F. Charbit, "Numerical Particle Tracking and Visualisation of Dean Vortices," 2nd Congress Tracers and Tracing Methods, Nancy, France, *Récent Progrés en Génie des Procédés, Tracers and Tracing Methods*, **15**(79), 17 (May 29–31, 2001).

Moll, R., P. Moulin, D. Veyret, and F. Charbit, "Numerical Simulation of Dean Vortices: Fluid Trajectories," *J. Memb. Sci.*, **197**, 157 (2002).

Mollet, L., P. Dumargue, M. Daguenet, and D. Bodiot, "Calcul du Flux Limite de Diffusion sur une Microélectrode de Section Circulaire," *Electrochim. Acta*, **19**, 841 (1974).

Moulin, P., J. C. Rouch, C. Serra, M. J. Clifton, and P. Aptel, "Mass Transfer Improvement by Secondary Flows: Dean Vortices in Coiled Tubular Membranes," *J. Memb. Sci.*, **114**, 235 (1996a).

Moulin, P., "Amélioration du Transfert de Matière dans les Opérations de Séparations par Membranes en Présence de Vortex de Dean," PhD Thesis, Université Paul Sabatier, Toulouse, France (1996b).

Moulin, P., P. Manno, J. C. Rouch, C. Serra, M. J. Clifton, and P. Aptel, "Flux Improvement by Dean Vortices: Ultrafiltration of Colloidal Suspensions and Macromolecular Solutions," *J. Memb. Sci.*, **109**, 156 (1999).

Moulin, P., D. Veyret, and F. Charbit, "Dean Vortices: Comparison of Numerical Simulation of Shear Stress and Improvement of Mass Transfer in Membrane Processes at Low Permeation Fluxes," *J. Memb. Sci.*, **183**, 149 (2001).

Park, J. Y., C. K. Choi, and J. J. Kim, "A Study on Dynamic Separation of Silica Slurry Using a Rotating Membrane Filter. I Experiments and Filtrate Fluxes," *J. Memb. Sci.*, **97**, 263 (1994).

Patankar, S. V., *Numerical Heat Transfer and Fluid Flow*, Hemisphere, New York (1980).

Reiss, L. P., and T. J. Hanratty, "An Experimental Study of the Unsteady Nature of a Viscous Sublayer," *AIChE J.*, **9**, 154 (1963).

Reiss, L. P., and T. J. Hanratty, "Measurement of Instantaneous Rates of Mass Transfer to a Small Sink on a Wall," *AIChE J.*, **8**, 245 (1962).

Sutey, A. M., and J. G. Knudsen, "Mass-Transfer at Solid-Liquid Interface for Climbing Film Flow in an Annular Duct," *AIChE J.*, **15**, 719 (1969).

Tanishita, K., P. D. Richardson, and P. M. Galleti, "Tightly Wound Coils of Microporous Tubing: Progress with Secondary Flow Blood Oxygenator Design," *Trans. Amer. Soc. Artific. Intern. Organs*, **21**, 216 (1975).

Wang, C. Y., "On the Low Reynolds-Number Flow in a Helical Pipe," *J. Fluid Mech.*, **108**, 185 (1981).

Wang, Y., J. A. Howell, R. W. Field, and D. Wu, "Simulation of Crossflow Filtration for Baffled Tubular Channels and Pulsatile Flow," *J. Memb. Sci.*, **95**, 243 (1994).

Winzeler, H. B., and G. Belfort, "Enhanced Performance for Pressure-Driven Membrane Processes: the Argument for Fluid Instabilities," *J. Memb. Sci.*, **80**, 35 (1993).

Wolff, M., and G. Cognet, "Etude Locale du Frottement Pariétal Dans un écoulement en Conduite Courbe," *J. Appl. Math. Physics*, **36**, 221 (1985).

Manuscript received Sept. 6, 2002, revision received Feb. 3, 2003 and final revision received Apr. 30, 2003.